

Multi-UAV Wildfire Perimeter Monitoring System

Constantinos Heracleous
KIOS CoE

University of Cyprus
Nicosia, Cyprus

heracleous.constantinos@ucy.ac.cy

Panayiotis Kolios
KIOS CoE

University of Cyprus
Nicosia, Cyprus

pkolios@ucy.ac.cy

Christos Panayiotou

KIOS CoE and Department of ECE
University of Cyprus

Nicosia, Cyprus
christosp@ucy.ac.cy

Abstract—Monitoring the perimeter of a wildfire in real time is crucial for effective firefighting and decision-making. This paper proposes a multi-UAV system that combines real-time infield data with a fire propagation model to accurately predict the state of the wildfire perimeter and improve fire prediction. To achieve this, a data fusion scheme is used to merge historical data with real-time measurements obtained from UAVs to update the fire propagation model. The model is then used to predict the future perimeter of the fire, which then guides the team of UAVs to track the perimeter more accurately. The system has been tested through simulation experiments, indicating its effectiveness in providing accurate real-time wildfire perimeter propagation information.

Index Terms—Autonomous aerial vehicles, drones, fires, path planning, real-time systems, remote monitoring

I. INTRODUCTION

Climate change has precipitated a multitude of adverse effects, including rising temperatures, prolonged droughts, and alterations in precipitation patterns. Consequently, wildfires' frequency, intensity, and unpredictability have significantly increased. The latest data from the recent EFFIS annual report [1] highlights this disturbing trend recording the highest number of fires since 2006, accompanied by the most severe drought experienced in Europe in the past 500 years.

Effectively combating wildfires necessitates early detection, precise propagation estimation, and continuous tracking [2]. Moreover, real-time information regarding the state of the wildfire is vital for situational awareness and informed decision-making when formulating appropriate action plans to suppress fire spread and implement evacuation procedures when deemed necessary [3].

Recently, the advent of unmanned aerial vehicles (UAVs) has significantly improved real-time wildfire monitoring capabilities. Compared to conventional methods like satellite image inspection or manned aerial vehicles such as helicopters, UAVs offer substantial advantages. They significantly reduce operational costs and minimize risks when compared to manned

This work has been supported by the RESTART 2016 – 2020 call for proposals for the Excellence Hubs Programme, Pillar II – Sustainable RTDI System through the Cyprus Research and Innovation Foundation under grant agreement EXCELLENCE/0421/0586 (GLIMPSE) Intelligent Multi-drone Emergency Response System. It is also supported by the European Union Civil Protection Call for proposals UCPM-2022-KN grant agreement No 101101704 (COLLARIS Network) and European Union's Horizon 2020 research and innovation program under grant agreement No 739551 (KIOS CoE - TEAMING) and from the Republic of Cyprus through the Deputy Ministry of Research, Innovation and Digital Policy.

aerial vehicles. Additionally, UAVs are readily available and equipped with a variety of sensors to provide immediate coverage, surpassing the periodic coverage and lengthy revisit times associated with satellite wildfire monitoring.

Over the past few years, a significant amount of research has been dedicated to using UAVs for tracking wildfire propagation. This has resulted in several methods being proposed and reviewed [4]–[7]. The concept of using UAVs for wildfire tracking was initially proposed in [2], which introduced a cooperative control method for monitoring the fire perimeter. By guiding a team of UAVs in clockwise and counterclockwise directions around the fire perimeter, this method aimed to minimize information latency and the frequency of updates to the mission base station. The fire perimeter tracking problem was also studied in [8], with the authors proposing cooperative control for a team of UAVs based on optimizing utility functions keeping the UAVs close to the fire boundary.

The authors in [9] have devised a coordination technique that prioritizes the monitoring of critical wildfire areas using a team of UAVs. They have implemented a method that directs the UAVs to visit high-importance perimeter points more frequently based on the fire's spread rate instead of monitoring the entire perimeter uniformly. In a similar vein, the authors in [10] have focused on monitoring the faster-moving segment of the fire frontier with UAVs, developing a sliding-mode control algorithm that optimizes the UAVs' movement towards the rapidly moving fire region.

In [3], a distributed control framework is proposed that allows a group of UAVs to monitor the spread of wildfires collaboratively. By minimizing data loss from the onboard



Fig. 1. The proposed multi-UAV system for wildfire perimeter monitoring that integrates the UAVs' sensing capabilities and a wildfire propagation model.

cameras and quantifying fire heat intensity levels, the UAVs can monitor the perimeter as it expands while ensuring complete wildfire coverage. The work in [11] proposed a similar framework but with additional consideration for areas of firefighter activity. The authors generate a fire-front uncertainty map and a human uncertainty map from GPS signals received by firefighters. By minimizing a dual-criteria objective function, they determine the positions that the UAVs must navigate to monitor the fire and sense the firefighters. Finally, in [12], the authors proposed a UAV-based system that monitors the wildfire progression while periodically flying ahead of the fire to collect valuable data that can aid in anticipating fire behavior and movement.

In comparison to the previous aforementioned approaches, in this work, we devise and propose a multi-UAV system that integrates the UAVs' sensing capabilities and a wildfire propagation model to provide real-time state information on the wildfire perimeter (see Fig. 1) further expanding our initial work in [13]. The proposed system enables a team of UAVs to navigate in specific wildfire perimeter segments so that the uncertainty of the fire propagation model is minimized and thus more accurately and efficiently track the fire perimeter. Specifically, the proposed system consists of UAVs measuring the fire perimeter, fuel type, and weather conditions. To improve the accuracy of wildfire perimeter monitoring, we use a data fusion scheme that combines historical data with real-time data from onboard sensors. This feeds into a wildfire propagation model, which generates real-time estimates of the future perimeter state. Our perimeter tracking scheme then calculates trajectories for UAVs to minimize the error between the anticipated and actual perimeter. Finally, a guidance and control scheme is utilized to ensure efficient navigation and measurement collection by the UAV team.

The rest of this paper is organized as follows. Section II discusses the wildfire propagation model utilized. Section III formulates the problem. Section IV details the proposed multi-UAV system for real-time wildfire perimeter propagation monitoring. Section V presents simulation results demonstrating the method's efficacy. Finally, Section VI offers some concluding remarks.

II. WILDFIRE MODELLING PRELIMINARIES

The forward model is utilized in this work for characterizing wildfire propagation mathematically. Specifically, based on [14], [15], we implement the wildfire forward model, a simplified version of the advanced FARSITE model [16], that requires fewer inputs but still represents a realistic surface fire propagation. The wildfire forward model can be described by the following discrete-time function:

$$q(t+1) = f(q(t), u(t)), \quad \forall t \geq 0 \quad (1)$$

where $q(t) = [q_1(t), \dots, q_{N(t)}(t)]^T$ denote the fire-front vertices in the 2D plane that represents the wildfire perimeter in a counterclockwise direction when they are connected together, with $q_1(t) = q_{N(t)}(t)$. The number of perimeter's fire-fronts in each time step is denoted with $N(t) \in \mathbb{Z}^+$, while $q(0) = q_0$

and $N(0) = N_0$ is the initial fire-front locations and number, respectively. The input $u(t) = [R(t), U(t), \theta(t)]$ consists of the matrices $R, U, \theta \in \mathbb{R}^{n_x \times n_y}$ where R denotes the steady-state of fire spread rate, which can be calculated using the Rothermel model [17] and the fuel characteristics, U is the mid-flame wind speed, and θ is the wind direction. Lastly, function $f(\cdot)$ includes the dynamical model and also the loop-clipping and discretization algorithms, which we describe in the sequel, and together calculate the wildfire perimeter propagation.

Specifically, the dynamical model utilizes Huygens' expansion-based approach to calculating the propagation of each fire front in the 2D plane using the following discrete-time dynamical model:

$$q_i(t+1) = q_i(t) + \Delta t Q_i(t), \quad \forall i = 1, \dots, N(t), \quad (2)$$

where $q_i = [x_i, y_i]^T$ are the cartesian coordinates of i -th fire-front vertex, while Δt is the time step. $Q_i = [X_i, Y_i]^T$ are the orthogonal spread rate differentials (m min^{-1}):

$$\begin{aligned} X_i &= \frac{a^2 c \theta (x_s \delta \theta + y_s c \theta) - b^2 \delta \theta (x_s c \theta - y_s \delta \theta)}{\sqrt{b^2 (x_s c \theta - y_s \delta \theta)^2 + a^2 (x_s \delta \theta + y_s c \theta)^2}} + c \delta \theta, \\ Y_i &= \frac{-a^2 \delta \theta (x_s \delta \theta + y_s c \theta) - b^2 c \theta (x_s c \theta - y_s \delta \theta)}{\sqrt{b^2 (x_s c \theta - y_s \delta \theta)^2 + a^2 (x_s \delta \theta + y_s c \theta)^2}} + c c \theta, \end{aligned} \quad (3)$$

where $c \theta$ and $\delta \theta$ is a shortened form for $\cos \theta$ and $\sin \theta$, respectively, while θ is the angle (rad, $0 \leq \theta < 2\pi$) of the wind direction measured from the positive y-axis in a clockwise direction. $x_s = x_{i+1} - x_{i-1}$ and $y_s = y_{i+1} - y_{i-1}$ denote the component differentials representing the orientation of the i -th vertex on the fire-front, while a, b and c (m min^{-1}) describe the shape of an elliptical fire at each vertex calculated as follows:

$$a = \frac{0.5(R + \frac{R}{HB})}{LB}, \quad b = \frac{(R + \frac{R}{HB})}{2}, \quad c = b - \frac{R}{HB} \quad (3)$$

where R is the fire spread rate (m min^{-1}), HB is the head to back ratio given as $HB = \frac{LB + (LB^2 - 1)^{0.5}}{LB - (LB^2 - 1)^{0.5}}$, and LB is the length to breadth ratio given as $LB = 0.936e^{0.2566U} + 0.461e^{-0.1548U} - 0.397$, with U denoting the the mid-flame wind speed (m s^{-1}).

Because of non-uniform inputs (i.e., rate of spread and weather), using only (2) to propagate each fire-front can generate internal loops in the perimeter representation rendering it illogical and unusable [16]. These loops need to be removed continuously using a loop-clipping filter. In this work, a loop-clipping algorithm has been implemented that checks at each time step if any perimeter segments intersect. It then removes them accordingly to avoid the development of internal loops and updates the number of fire-front vertices, i.e., $N(t)$.

Another problem that arises when using (2) is that as the perimeter expands, there is an increase in distance between the fire-front vertices. This results in an erroneous perimeter representation. To eliminate this error, a discretization algorithm has been implemented that adds new vertices to the perimeter

sections with high curvature. The following condition is used for determining where to add new vertices [14]:

$$\max\left(\cos\frac{\beta_i}{2}, \cos\frac{\beta_{i-1}}{2}\right) > \left(\frac{\Omega}{\ell_i}\right)^2, \quad (4)$$

where β_i (or β_{i-1}) is the angle between the segments of vertices q_{i+1}, q_i, q_{i-1} (or q_i, q_{i-1}, q_{i-2}). $\ell_i = \|q_i - q_{i-1}\|$ is the distance between the subsequent vertices q_i and q_{i-1} , and Ω is a positive user specified threshold parameter. If the condition in (4) is true in any line segment of the perimeter, then a new vertex is added at the midpoint of that segment (i.e., $\frac{\ell_i}{2}$), and the number of the fire-front vertices, i.e., $N(t)$ is updated accordingly. The algorithm runs recursively to the newly generated segment halves, and new vertices are added until the condition in (4) is satisfied by all the perimeters segments.

III. PROBLEM FORMULATION

In an area affected by a wildfire, we aim to deploy a team of UAVs or drones equipped with appropriate measurement sensors. These UAVs must gather real-time data, which are then used with a simulated wildfire model to provide continuous updates on the current state of the fire perimeter.

Definition 1 (Wildfire Perimeter). *We consider the true wildfire perimeter as a dynamic set of fire-front vertices $q(t) = [q_1(t), \dots, q_{N(t)}(t)]^T$ connected in a counter-clockwise direction in the 2D plane and propagate using (1) as described in Section II.*

Definition 2 (UAVs). *A homogeneous team of UAVs $\mathcal{D} = \{\mathcal{D}_1, \dots, \mathcal{D}_M\}$ can be deployed to monitor and gather real-time data from the wildfire. The position of the \mathcal{D}_j UAV is represented in the 3D space: $p_j = [x_j, y_j, z_j]^T \in \mathbb{R}^3$, where $[x, y] \in \mathbb{R}^2$ denotes the 2D plane coordinates while $z \in \mathbb{R}$ denotes the altitude. Also, its movement in the 3D space is represented by the discrete-time linear dynamical model:*

$$p_j(t+1) = p_j(t) + v_j(t)\Delta t, \quad (5)$$

where Δt is the time step and $v_j \in \mathbb{R}^3$ is the control input that is represented by the speed vector $v_j = [v_j^x, v_j^y, v_j^z]^T$

The UAVs are equipped with a hyperspectral camera mounted on the underside, complemented by advanced software that enables measurement of the fire perimeter and the fire's spread rate through identifying the area fuel types (i.e., vegetation) [18]. As shown in Fig. 2, the camera has a square field of view (FOV), with side length l given by:

$$l_j(t) = 2z_j(t) \tan\frac{\varphi}{2}, \quad (6)$$

where $z_j \in p_j$ is the \mathcal{D}_j UAV altitude, and $\varphi = 2 \tan^{-1} \frac{S}{2F}$ is the angular FOV with S denoting the sensor size, and F is the lens focal length both available from the camera specifications. In addition, every UAV is fitted with a wind and weather sensor (WWS) that enables the measurement of wind speed and direction while flying in 3D space. Therefore, each \mathcal{D}_j UAV through its onboard sensors acquires the following real-time

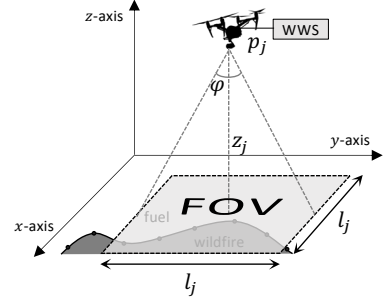


Fig. 2. Each UAV, through its onboard sensors and relative to its position and FOV, can measure the wildfire perimeter, rate of spread, and wind speed and direction.

measurement vector relative to its position $p_j(t)$ and FOV: $[q_m(t), R_m(t), U_m(t), \theta_m(t)]$ that consists of measurements for the fire-front position $q_m(t)$, the fire spread rate $R_m(t)$, the wind speed $U_m(t)$ and wind direction $\theta_m(t)$.

Definition 3 (Simulated Wildfire Perimeter). *The simulated wildfire perimeter is represented by the dynamic set of fire-front vertices $\hat{q}(t) = [\hat{q}_1(t), \dots, \hat{q}_{\hat{N}(t)}(t)]^T$ connected in a counter-clockwise direction in the 2D plane. The simulated wildfire also propagates using (1), with $\hat{q}(0) = q(0)$. However, the input matrices used are obtained from historical data of the area (i.e., $u = u_d = [R_d, U_d, \theta_d]$) or fused data, which combines historical data with real-time data from the UAVs (i.e., $u = u_f = [R_f, U_f, \theta_f]$).*

Problem 1 (Wildfire Perimeter Monitoring). *Given an area affected by a wildfire with perimeter $q(t)$ and imprecise area historical data for simulating the wildfire perimeter $\hat{q}(t)$, devise a system that guides a team of M UAVs to specific locations for real-time measurements that will not only depict the growing fire perimeter but also update the model in order to further more accurately predict the future fire perimeter and more appropriately guide the UAVs to their next locations.*

To assess the performance of the proposed system, we consider the overall mean error distance between the true wildfire perimeter $q(t)$ and the simulated wildfire perimeter $\hat{q}(t)$ over a period T given by

$$E_d = \frac{1}{T} \sum_{t=1}^T \varepsilon_d(t), \quad (7)$$

where $\varepsilon_d(t)$ is the mean error distance between $q(t)$ and $\hat{q}(t)$ at time t , i.e.,

$$\varepsilon_d(t) = \frac{1}{N_d(t)} \sum_{i=1}^{N_d(t)} d_i(t), \quad (8)$$

where $d_i, i = 1, \dots, N_d$ is the i -th Euclidian distance between wildfire and simulated perimeter segments. These distances are computed by initially finding the midpoints $\hat{\kappa}$ in between the simulated perimeter fire-front vertices, i.e., $\hat{\kappa}_i = \frac{\hat{q}_i + \hat{q}_{i+1}}{2}$,

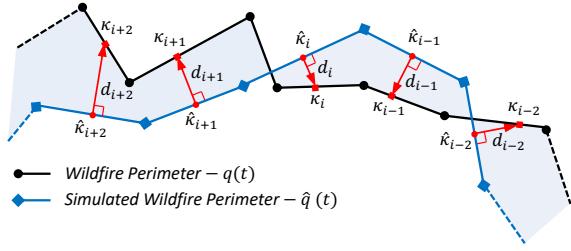


Fig. 3. Distance illustration between wildfire perimeter $q(t)$ (black line) and wildfire simulated perimeter $\hat{q}(t)$ (blue line). Red arrows are Euclidean distances d between true and simulated perimeters, red circles are the midpoints $\hat{\kappa}$, and red squares are the perpendicular intersection points κ .

and then the points κ in the corresponding wildfire perimeter determined by the perpendicular intersection from each $\hat{\kappa}_i$ point, as depicted in Fig. 3 [19]. Finally, each Euclidean distance d_i can be computed by $d_i = \|\hat{\kappa}_i - \kappa_i\|$.

IV. PROPOSED SYSTEM ARCHITECTURE

The proposed system is illustrated in Fig. 4, which consists of four interconnected modules that we describe in the following paragraphs.

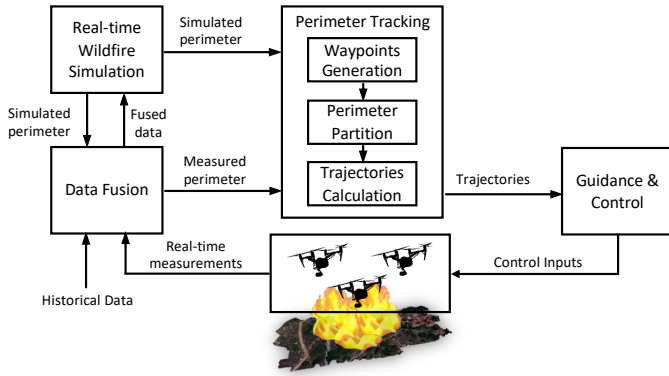


Fig. 4. Overview of the proposed multi-UAV wildfire perimeter monitoring system architecture.

A. Real-time Wildfire Simulation

The proposed system utilizes the wildfire model described in Section II to simulate the wildfire perimeter in real-time using fused historical data and UAV real-time measurements after their processing by the Data Fusion (DF) module (see Section IV-B). Specifically, the following discrete-time dynamical model is used, similar to (1):

$$\hat{q}(t+1) = f(\hat{q}_f(t), u_f(t)), \quad (9)$$

where $\hat{q}(t) = [\hat{q}_1(t), \dots, \hat{q}_{\hat{N}(t)}(t)]^T$ are the simulated fire-front perimeter vertices, while $\hat{q}_f(t)$ are the fused perimeter vertices and $u_f(t) = [R_f(t), U_f(t), \theta_f(t)]$ are the fused input matrices available from DF module. The system output is the simulated wildfire perimeter $\hat{q}(t)$ and is provided to the firefighting mission commander.

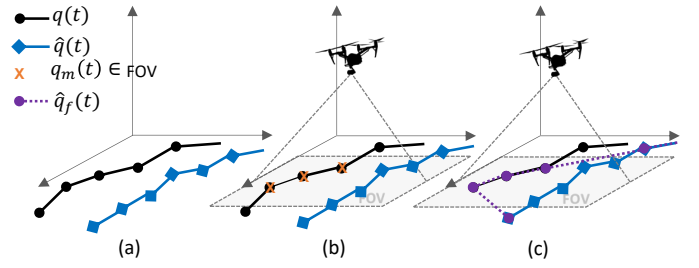


Fig. 5. Data fusion module process for a perimeter segment.

B. Data Fusion

The DF module fuses historical data with infield measurements from the UAVs to enhance real-time wildfire simulation and, subsequently UAV guidance accuracy.

Specifically, the historical data matrices for fire spread rate (R_d), wind speed (U_d), and wind direction (θ_d), as well as real-time measurements ($R_m(t)$, $U_m(t)$, $\theta_m(t)$) obtained by the UAV are fused through the DF module. Firstly, the fused matrices are initialized with the available historical data, i.e., $R_f = R_d$, $U_f = U_d$, $\theta_f = \theta_d$. After the UAVs are deployed, the fused matrices are continually updated with real-time measurements based on the UAVs' positions ($p_1(t), \dots, p_M(t)$). In other words, the real-time measurements for fire spread rate ($R_m(t)$), wind speed ($U_m(t)$), and wind direction ($\theta_m(t)$) are mapped according to each UAV position and added to their respective fused matrices (R_f , U_f , θ_f). This results in an updated spatial-temporal input vector ($u_f = [R_f, U_f, \theta_f]$) that is used in (9).

The DF module also fuses the simulated wildfire with real-time perimeter measurements from the UAVs. The process is depicted in Fig. 5. In particular, Fig. 5(a) illustrates segments of the true perimeter $q(t)$ and the simulated perimeter $\hat{q}(t)$ before the arrival of the UAV. After the arrival of the UAV (see Fig. 5(b)), the true fire-front vertices are identified and measured and then fused with the already available perimeter measurements $q_m(t)$. Subsequently, the fire-front measurements $q_m(t) \in \text{FOV}$ are fused with the simulated perimeter $\hat{q}(t)$ to obtain the fused simulated perimeter $\hat{q}_f(t)$ as shown in Fig. 5(c). The process repeats for all the UAVs in the team, providing the fused simulated perimeter $\hat{q}_f(t)$ that is used in (9). Data fusion is essential to the system since it provides continuously available real-time measurements for the perimeter state and necessary inputs that improve the accuracy of wildfire simulation.

C. Perimeter Tracking

The PT module is responsible for calculating trajectories for all the UAVs in the team. These trajectories are denoted by $\mathcal{T} = \{\mathcal{T}_1, \dots, \mathcal{T}_M\}$, and they are computed based on each UAV position in the 3D space and the distance between the simulated perimeter $\hat{q}(t)$ and the measured perimeter $q_m(t)$. Each trajectory $\mathcal{T}_j = [w_1, \dots, w_{N_w}]$ represents the calculated path for the UAV \mathcal{D}_j and consists of waypoints $w_i = [x_i, y_i, z_i]$ that the UAV needs to track. Initially, PT

computes the trajectories when a UAV reaches the wildfire perimeter. Then, new trajectories are computed if any UAV in the team reaches the final waypoint of its current trajectory.

PT utilizes Algorithm 1 for computing the trajectories. To explain the process, Algorithm 1 is divided into three parts: Waypoints Generation, Perimeter Partition, and Trajectories Calculation. Additionally, Fig. 6 visually represents the tasks involved in generating waypoints and partitioning.

Algorithm 1 Perimeter Tracking

```

1: Input:  $\hat{q}(t), q_m(t), p_1(t) \dots p_M(t)$ 
2: Output:  $\mathcal{T} = \{\mathcal{T}_1, \dots, \mathcal{T}_M\}$ 
3: if  $\mathcal{D}_j$  reaches final waypoint  $w_{N_w} \in \mathcal{T}_j$  then
4:    $[W, d^m] \leftarrow \text{waypointsGeneration}(\hat{q}(t), q_m(t))$ 
5:    $[R_1, \dots, R_M] \leftarrow \text{perimeterPartition}(W, p_1(t) \dots p_M(t))$ 
6:    $A \leftarrow \text{generateAdjacencyMatrix}(W)$ 
7:   for each UAV  $\mathcal{D}_j$  do
8:      $w_S \leftarrow \text{findStartWaypoint}(p_j(t), R_j)$ 
9:      $w_E \leftarrow \text{findEndWaypoint}(p_j(t), R_j, d^m)$ 
10:     $\mathcal{T}_j \leftarrow \text{dijkstra}(A, w_S, w_E)$ 
11:   end for
12: end if
  
```

1) *Waypoints Generation:* To generate the waypoints, we first calculate the distances d_i^m , $i = 1, \dots, N_d^m$ between the simulated perimeter $\hat{q}(t)$ and the measured perimeter $q_m(t)$. This is done in a similar manner as explained in Section III for calculating the distances d_i . Next, we compute the waypoints set W by using the 2D coordinates of $\hat{\kappa}^m$ (which are the intersection points of the perpendicular line extended from κ^m points, much like explained in Section III for κ and $\hat{\kappa}$ points, respectively) at an altitude z_i . Therefore, each waypoint $w_i \in W$ is denoted by $w_i = [\hat{\kappa}_i^m, z_i]$. The altitude is found based on (6), which ensures that the FOV of the UAV adequately covers both $\hat{q}(t)$ and $q_m(t)$ perimeters:

$$z_i = \frac{2s d_i^m}{\tan \frac{\varphi}{2}}, \quad (10)$$

where $s \geq 1$ is a user-defined scaling factor parameter.

2) *Perimeter Partitioning:* By utilizing the set of waypoints W and the current positions of the UAVs, i.e., $p_1(t) \dots p_M(t)$,

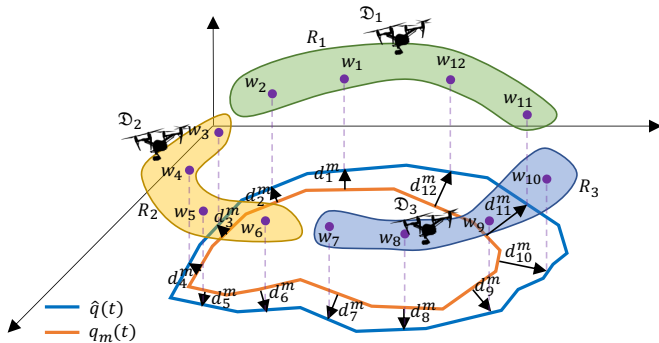


Fig. 6. Waypoints generation and perimeter partition into regions.

the perimeter can be partitioned into M regions, denoted as R_1, \dots, R_M , which corresponds to the number of UAVs in the team. An example is illustrated in Fig. 6. Each region, denoted as R_j , contains the waypoints that are nearer to UAV \mathcal{D}_j , and can be determined using:

$$R_j = \{w \mid \|\lambda(w, p_j(t))\| \leq \|\lambda(w, p_i(t))\|, \forall j \neq i\}, \quad (11)$$

where, $\lambda(w, p_j(t))$ represents the length distance from the position $p_j(t)$ of UAV \mathcal{D}_j to any waypoint $w \in W$ while considering passing through the intermediate waypoints.

3) *Trajectories Calculation:* In order to determine the trajectory of each UAV, we begin by creating an adjacency matrix A based on a set of waypoints W . The matrix is sparse since it only includes connections between adjacent waypoints, with the distance between them acting as a weight ($d_i = \|w_{i+1} - w_i\|$). This ensures that the UAVs remain outside the wildfire and only fly along its perimeter. We then determine the starting and ending waypoints for each UAV \mathcal{D}_j . The starting waypoint w_S is the closest waypoint within the UAV \mathcal{D}_j monitoring area R_j , i.e.,

$$w_S = \arg \min_{w \in R_j} \|p_j(t) - w\| \quad (12)$$

The ending waypoint w_E for \mathcal{D}_j is the waypoint within its monitoring area R_j associated with the largest distance d^m . Finally, we calculate the trajectory \mathcal{T}_j for each UAV using Dijkstra's shortest path algorithm. We use the adjacency matrix A , with the starting waypoint w_S as the initial node and the ending waypoint w_E as the final node. This process is repeated for all the UAVs in the team.

D. Guidance and Control

Algorithm 2 Guidance and Control

```

1: Input:  $\mathcal{T}_j = [w_1, \dots, w_{N_w}], p_j(t)$ 
2: Output:  $v_j(t) = [v_j^x(t), v_j^y(t), v_j^z(t)]^T$ 
3:  $i \leftarrow 1$ 
4:  $\epsilon \leftarrow V_{\text{ref}} \Delta t$ 
5: while  $\|p(t) - w_{N_w}\| > \epsilon$  do
6:   if  $\|p_j(t) - w_i\| \leq \epsilon$  then
7:      $i \leftarrow i + 1$ 
8:   end if
9:    $d_w(t) \leftarrow w_i - p_j(t)$ 
10:   $\phi(t) \leftarrow \tan^{-1}(\frac{d_w^y(t)}{d_w^x(t)})$ 
11:   $\theta(t) \leftarrow \tan^{-1}(\frac{\sqrt{(d_w^x(t))^2 + (d_w^y(t))^2}}{d_w^z(t)})$ 
12:   $v_j^x(t) = V_{\text{ref}} \cos \phi(t) \sin \theta(t)$ 
13:   $v_j^y(t) = V_{\text{ref}} \sin \phi(t) \sin \theta(t)$ 
14:   $v_j^z(t) = V_{\text{ref}} \cos \theta(t)$ 
15: end while
  
```

The Guidance and Control (GC) module is responsible for providing the necessary control inputs to each UAV in the team so that they follow the computed trajectories. Algorithm 2 is utilized by the GC for each $\mathcal{D}_j \in \mathcal{D}$. Specifically, at each time step, GC computes the distance in each dimension

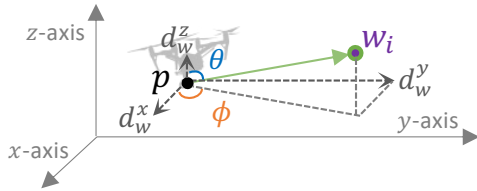


Fig. 7. 3D polar coordinates system.

(i.e., d_w^x, d_w^y, d_w^z as shown in Fig. 7) between the current position $p_j(t)$ of UAV \mathcal{D}_j and the waypoint $w_i \in \mathcal{F}_j$ that must be reached, via $d_w(t) = w_i - p_j(t)$. Using the 3D polar coordinates system displayed in Fig. 7, GC calculates the horizontal azimuth angle $\phi(t)$ measured on the xy plane from the x -axis (Alg. 2-line 10) and the azimuth angle $\theta(t)$ measured from the z axis (Alg. 2-line 11). Finally, the control speed vector is determined by computing the speed in each dimension (Alg. 2-lines 12-14) using the reference speed V_{ref} set by the user. A UAV \mathcal{D}_j is deemed to have reached a waypoint $w_i \in \mathcal{F}_j$ when $\|p_j(t) - w_i\| \leq \epsilon$, where $\epsilon = V_{\text{ref}}\Delta t$ is the distance error threshold. If a UAV in the team reaches its last waypoint $w_{N_w} \in \mathcal{F}_j$, then the calculation of new trajectories for all the UAVs in the team is triggered.

V. SIMULATION RESULTS

We conducted simulation experiments in the Matlab environment to evaluate the proposed system. The simulation outcomes were obtained using the parameter values specified in Table I. In order to have various fire shapes to assess the proposed system, the grid $G \times G$ is divided into a random number of cells. Subsequently, a rate of spread value is assigned to each cell from a normal distribution where the mean value μ_R takes values between 0-120m/min. Also, the wind direction changes over time through the simulation (see Table I). In all the simulations, the wildfire starts around [10km, 10km] while the UAVs are deployed from a depot at [11.5km, 11.5km]. The first UAV was deployed two minutes after the start of the fire, followed by subsequent UAVs every minute. Lastly, as indicated in Table I, we considered three scenarios for the available historical data. In Scenario A, the historical data values (i.e., R_d, U_d, θ_d) were underestimated by 40% from the actual values (i.e., R, U, θ). In Scenario B, the historical data values were close-estimated by 5% from the actual values, and finally, in Scenario C, the historical data values were over-estimated by 40% from the actual values.

The first simulation results presented in Fig. 8 demonstrate how the proposed system guides a team of three UAVs to monitor the wildfire perimeter. The results of a single simulation run are examined, displaying snapshots every 10 minutes of the movements of the three UAVs while monitoring the wildfire perimeter as it spreads. In all snapshots, it is evident that the three UAVs consistently keep track of the wildfire perimeter, adjusting their altitudes as necessary to always keep the perimeter within their field of view.

TABLE I
SIMULATION PARAMETERS VALUES

General	
Time step: $\Delta t = 5s$	Simulation time: $T = 120min$
Wildfire Model Parameters	
Grid size [$G \times G$]: $G = 25km$	Rediscret. threshold: $\Omega = 50m$
Grid resolution: 1m	
Initial fire-fronts: $N_0 = 80$	Wind direction (rad):
Initial position: [10km, 10km]	$\theta(t) \sim \mathcal{N}(\mu_\theta(t), \sigma_\theta(t) = \frac{\pi}{36})$
Rate of spread (m min ⁻¹):	$\mu_\theta(0 \leq t < 30) = \frac{\pi}{4}$
$R \sim \mathcal{N}(\mu_R=0-120, \sigma_R = 0.1\mu_R)$	$\mu_\theta(30 \leq t < 60) = \frac{19}{12}\pi$
Wind speed (m s ⁻¹):	$\mu_\theta(60 \leq t < 90) = \frac{5}{12}\pi$
$U \sim \mathcal{N}(\mu_U = 2, \sigma_U = 0.2)$	$\mu_\theta(t \geq 90) = \frac{5}{36}\pi$
UAVs Parameters	
Initial position [km]:	Deploy time of \mathcal{D}_j : $t_j = jmin$
$p_j(0) = [11.5, 11.5, 0]$	Reference speed: $V_{\text{ref}} = 15m/s$
Sensor size: $S = 24mm$	Lens focal length: $F = 24mm$
Scaling factor: $s = 2$	
Historical Data	
Scenario A (under-estimated -40%): $R_d=0.6R, U_d=0.6U, \theta_d=0.6\theta$	
Scenario B (close-estimated 5%): $R_d=1.05R, U_d=1.05U, \theta_d=1.05\theta$	
Scenario C (over-estimated 40%): $R_d=1.4R, U_d=1.4U, \theta_d=1.4\theta$	

Fig. 9 shows the outcomes of 1500 simulation runs that compare the effectiveness of the suggested system with varying accuracy levels of historical data and the number of UAVs. Specifically, a total of 50 simulations are run for each number of UAVs, with a total of 250 for each scenario computing the overall mean error of the simulated wildfire as given in (7). For direct comparison, we also included the overall mean error of the simulated wildfire using only the historical data and the overall mean error of the measured wildfire by the UAVs. As can be seen from the results, the performance of the proposed system is better in all scenarios and the number of UAVs. In Figs. 9(a)&(c) where the accuracy of the historical data is compromised, the error in the perimeter provided by the proposed system is significantly lower compared to the perimeter obtained by using historical data only. In Fig. 9(b), where the accuracy of the historical data is close to the true values, we can still observe that the proposed system still provides less erroneous wildfire perimeter. From the results, we can also observe that the proposed system's overall mean error improves when additional UAVs are utilized. Notably, it is also more effective than relying solely on perimeter measurements from UAVs since more UAVs are necessary to match the proposed system performance. This indicates that the proposed system is a resource-efficient solution that can free up resources for other tasks or future use and redundancy.

Finally, Fig. 10 presents the mean error of the proposed system as given in equation (8), with regards to the length of the wildfire perimeter and the number of UAVs employed. The outcomes are derived from the same simulation results mentioned earlier. As can be observed, in all scenarios, the

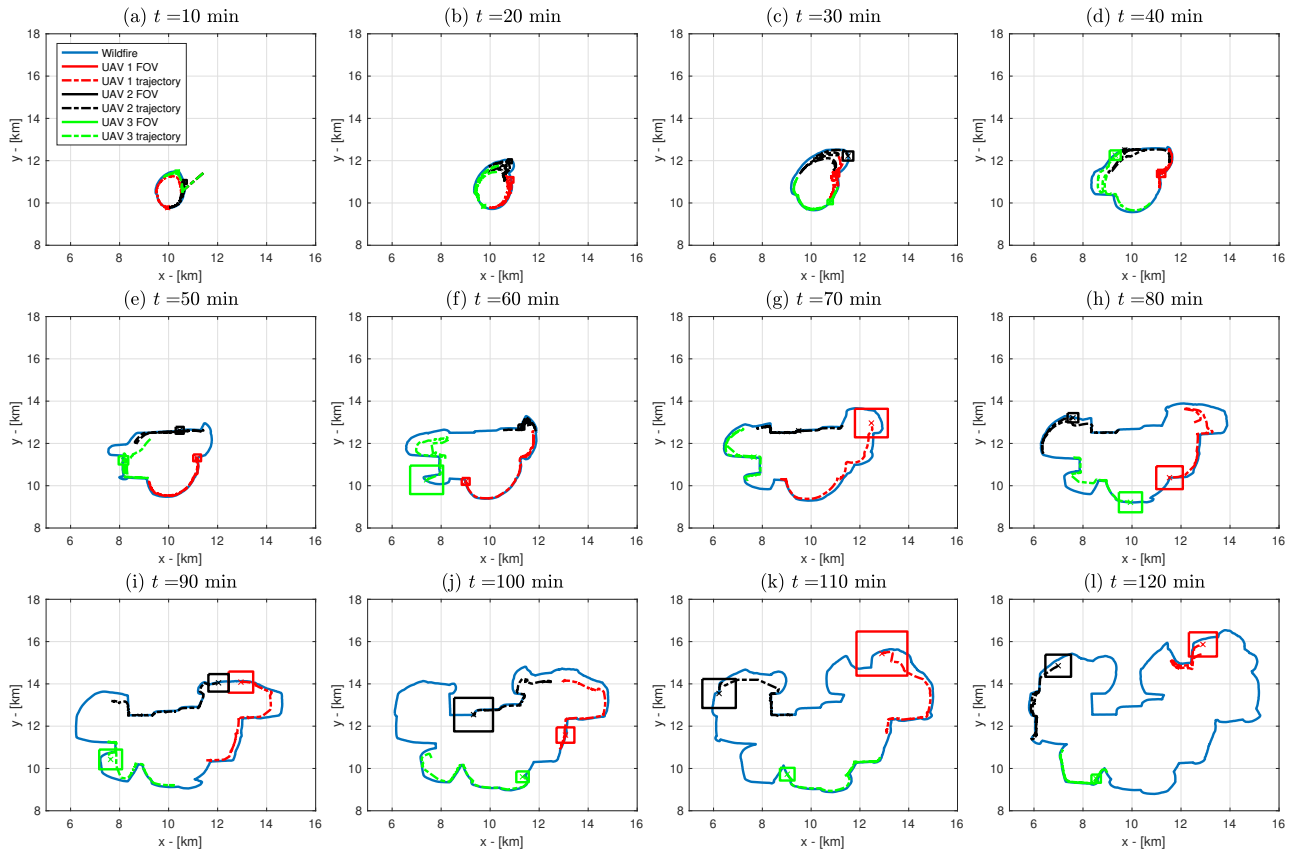


Fig. 8. Snapshots of the proposed system guiding a team of three UAVs to monitor the wildfire perimeter propagation in 10min time-steps. The FOV and the trajectory of each UAV are shown in each snapshot.

mean error is proportional to the length of the perimeter. However, using more UAVs improves the error as the perimeter increases.

VI. CONCLUSION AND FUTURE WORK

In this work, we propose a multi-UAV system that combines the sensing capabilities of a team of UAVs along with a wildfire propagation model to provide the real-time state of the wildfire perimeter. As described, the proposed system guides a team of UAVs capable of measuring the fire perimeter, fuel type, and weather conditions. A wildfire model is used for providing real-time simulations of the perimeter state. The simulation perimeter values, together with the UAVs' perimeter measurements, are used by the perimeter tracking scheme for calculating trajectories that minimize the error between the wildfire perimeter and the simulated perimeter. A guidance and control scheme guides the UAVs to follow the calculated trajectories and receive measurements. Lastly, a data fusion scheme fuses available historical data with real-time measurements providing updated inputs to the wildfire model, improving its performance. The proposed system is evaluated in a simulation environment showcasing its ability to monitor the wildfire perimeter and provide accurate perimeter state information.

In the future, we aim to evaluate the system using data from actual wildfire events. Furthermore, we would like to explore the possibility of adding and removing UAVs from the monitoring team in a dynamic manner, taking into account the battery limitations of each UAV. Moreover, communication challenges that UAVs face in real-world scenarios and the impact of adverse weather conditions on UAV operations will also be evaluated to improve the proposed system's robustness and practical applicability in real wildfire situations.

REFERENCES

- [1] J. San-Miguel-Ayanz, T. Durrant, R. Boca, P. Maianti, G. Liberta, T. Artes-Vivancos, D. Oom, A. Branco, D. de Rigo, D. Ferrari, H. Pfeiffer, R. Grecchi, D. Nuijten, M. Onida, and P. Loffler, "Forest Fires in Europe, Middle East and North Africa 2021," *Publications Office of the European Union, Luxembourg, JRC130846*, 2022.
- [2] D. W. Casbeer, D. B. Kingston, R. W. Beard, and T. W. McLain, "Cooperative forest fire surveillance using a team of small unmanned air vehicles," *International Journal of Systems Science*, vol. 37, no. 6, pp. 351–360, 2006.
- [3] H. X. Pham, H. M. La, D. Feil-Seifer, and M. C. Deans, "A Distributed Control Framework of Multiple Unmanned Aerial Vehicles for Dynamic Wildfire Tracking," *IEEE Transactions on Systems, Man, and Cybernetics: Systems*, vol. 50, no. 4, pp. 1537–1548, 2020.
- [4] C. Yuan, Y. Zhang, and Z. Liu, "A survey on technologies for automatic forest fire monitoring, detection, and fighting using unmanned aerial vehicles and remote sensing techniques," *Canadian Journal of Forest Research*, vol. 45, no. 7, pp. 783–792, 2015.

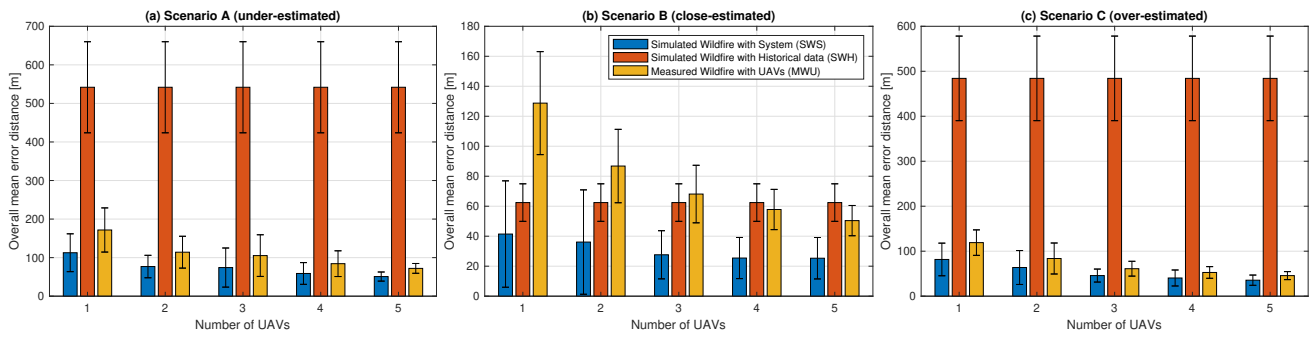


Fig. 9. The proposed system performance with different accuracy available historical data and number of UAVs. Fig. 9(a) the proposed system uses Scenario A under-estimated data, Fig. 9(b) the proposed system uses Scenario B close-estimated data, and Fig. 9(c) the proposed system uses Scenario C over-estimated data. For direct comparison, we present the overall mean error of (1) the simulated wildfire using the proposed system (SWS), the simulated wildfire using the historical data (SWH), and (3) the measured wildfire by the UAVs (MWU).

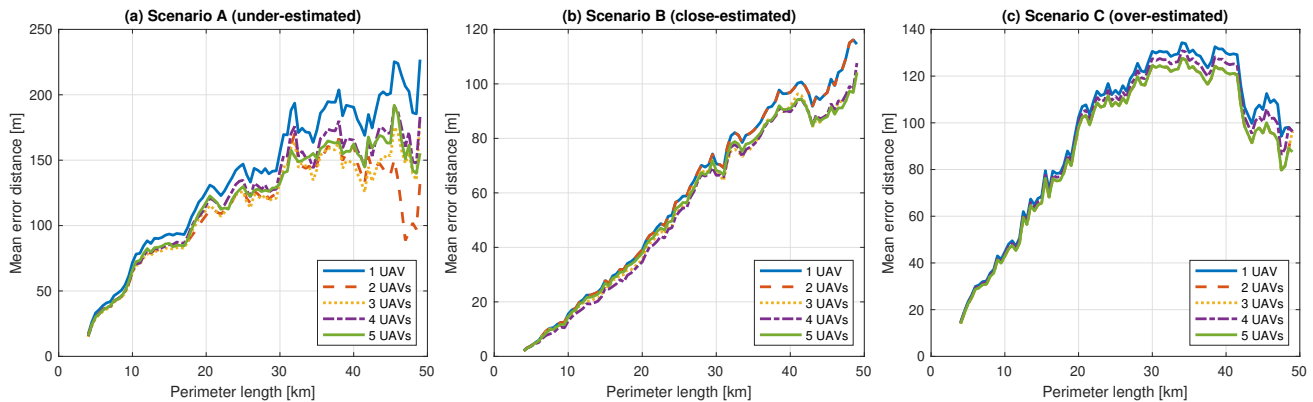


Fig. 10. The proposed system performance over the wildfire perimeter length and number of UAVs. Fig. 10(a) the proposed system uses Scenario A under-estimated data, Fig. 10(b) the proposed system uses Scenario B close-estimated data, and Fig. 10(c) the proposed system uses Scenario C over-estimated data.

[5] C. Torresan, A. Berton, F. Carotenuto, S. F. Di Gennaro, B. Gioli, A. Matese, F. Miglietta, C. Vagnoli, A. Zalzei, and L. Wallace, "Forestry applications of UAVs in Europe: a review," *International Journal of Remote Sensing*, vol. 38, no. 8-10, pp. 2427–2447, 2017.

[6] F. A. Hossain, Y. Zhang, and C. Yuan, "A Survey on Forest Fire Monitoring Using Unmanned Aerial Vehicles," in *2019 3rd International Symposium on Autonomous Systems (ISAS)*, 2019, pp. 484–489.

[7] M. A. Akhlofi, A. Couturier, and N. A. Castro, "Unmanned Aerial Vehicles for Wildland Fires: Sensing, Perception, Cooperation and Assistance," *Drones*, vol. 5, no. 1, p. 15, 2021.

[8] M. Kumar, K. Cohen, and B. HomChaudhuri, "Cooperative Control of Multiple Uninhabited Aerial Vehicles for Monitoring and Fighting Wildfires," *Journal of Aerospace Computing, Information, and Communication*, vol. 8, no. 1, pp. 1–16, 2011.

[9] X. Hu, J. Bent, and J. Sun, "Wildfire Monitoring with Uneven Importance Using Multiple Unmanned Aircraft Systems," in *2019 International Conference on Unmanned Aircraft Systems (ICUAS)*, 2019, pp. 1270–1279.

[10] A. V. Savkin and H. Huang, "Navigation of a Network of Aerial Drones for Monitoring a Frontier of a Moving Environmental Disaster Area," *IEEE Systems Journal*, vol. 14, no. 4, pp. 4746–4749, 2020.

[11] E. Seraj and M. Gombolay, "Coordinated Control of UAVs for Human-Centered Active Sensing of Wildfires," in *2020 American Control Conference (ACC)*, 2020, pp. 1645–1652.

[12] C. Heracleous, P. Kolios, and C. G. Panayiotou, "An integrated UAV system for wildfire evolution monitoring and data acquisition," in *2022 International Conference on Unmanned Aircraft Systems (ICUAS)*, 2022, pp. 1131–1138.

[13] —, "UAV-based system for real-time wildfire perimeter propagation tracking," in *2023 31st Mediterranean Conference on Control and Automation (MED)*, 2023, pp. 13–18.

[14] G. D. Richards, "An elliptical growth model of forest fire fronts and its numerical solution," *International Journal for Numerical Methods in Engineering*, vol. 30, pp. 1163–1179, 10 1990.

[15] P. L. Andrews, "The Rothermel surface fire spread model and associated developments: A comprehensive explanation," RMRS-GTR-371. Fort Collins, CO: U.S. Department of Agriculture, Forest Service, Rocky Mountain Research Station, Tech. Rep., 2018.

[16] M. A. Finney, "FARSITE: Fire Area Simulator—model development and evaluation," *Research Paper RMRS-RP-4 Revised*, 2004, Ogden, UT: U.S. Dept. Agric., Forest Service, Rocky Mountain Res. Station.

[17] R. C. Rothmel, "A Mathematical Model for Predicting Fire Spread in Wildland Fuels," *Washington, DC, USA: Intermountain Forest Range Exp. Station, Forest Service*, vol. 115, p. 46, 1972.

[18] J. H. Scott and R. E. Burgan, "Standard fire behavior fuel models: a comprehensive set for use with Rothermel's surface fire spread model," RMRS-GTR-153. Fort Collins, CO: U.S. Department of Agriculture, Forest Service, Rocky Mountain Research Station., Tech. Rep., 2005.

[19] O. Rios, E. Pastor, M. M. Valero, and E. Planas, "Short-term fire front spread prediction using inverse modelling and airborne infrared images," *International Journal of Wildland Fire*, vol. 25, p. 1033, 2016.